Hindawi
Advances in High Energy Physics
Volume 2017, Article ID 2864784, 14 pages
https://doi.org/10.1155/2017/2864784

Research Article

Dynamical System Analysis of Interacting Hessence Dark Energy in $f(T)$ Gravity

Jyotirmay Das Mandal and Ujjal Debnath

Department of Mathematics, Indian Institute of Engineering Science and Technology, Shibpur, Howrah 711 103, India

Correspondence should be addressed to Ujjal Debnath; ujjaldebnath@yahoo.com

Received 24 January 2017; Revised 31 March 2017; Accepted 15 May 2017; Published 25 July 2017

Academic Editor: George Siopsis

We have carried out dynamical system analysis of hessence field coupling with dark matter in $f(T)$ gravity. We have analysed the critical points due to autonomous system. The resulting autonomous system is nonlinear. So, we have applied the theory of nonlinear dynamical system. We have noticed that very few papers are devoted to this kind of study. Maximum works in literature are done treating the dynamical system as done in linear dynamical analysis, which are unable to predict correct evolution. Our work is totally different from those kinds of works. We have used nonlinear dynamical system theory, developed till date, in our analysis. This approach gives totally different stable solutions, in contrast to what the linear analysis would have predicted. We have discussed the stability analysis in detail due to exponential potential through computational method in tabular form and analysed the evolution of the universe. Some plots are drawn to investigate the behaviour of the system *(this plotting technique is different from usual phase plot and that devised by us)*. Interestingly, the analysis shows that the universe may resemble the "cosmological constant" like evolution (i.e., ΛCDM model is a subset of the solution set). Also, all the fixed points of our model are able to avoid Big Rip singularity.

1. Introduction

High end cosmological observations of the Supernova of type Ia (SN Ia), WMAP, and so forth [1–19] suggest the fact that the universe may be accelerating lately again after the early phase. Many theories are formulated to explain this late time acceleration. However, these theories can be divided mainly into two categories fulfilling the criteria of a homogeneous and isotropic universe. The first kind of theory (better to known as "standard model" or ΛCDM model) assumes a fluid of negative pressure named as "dark energy" (DE). The name arises from the fact the exact origin of this energy is still unexplained in theoretical setup. Observations, anyway, indicate that nearly 70% of the universe may be occupied by this kind of energy. Dust matter (cold dark matter (CDM) and baryon matter) comprises the remaining 30% and there is negligible radiation. Cosmologists are inclined to suspect dark energy as the primal cause of the late acceleration of universe. Theory of dark energy has remained one of the foremost areas of research in cosmology till the discovery of acceleration of the universe at late times [20–25]. One could clearly notice from the second field equation that the expansion would be accelerated if the equation of state (EoS) parameter satisfies $p/\rho \equiv \omega < -1/3$. Accordingly, a priori choice for dark energy is a time-independent positive "cosmological constant" which relates to the equation of state (EoS) $\omega = -1$. This gives a universe which is expanding forever at exponential rate. Anyway, cosmological constant has some severe shortcomings like fine tuning problem and so forth (see [20] for a review); some recent data [26, 27] in some sense agrees with this choice. By the way, observation which constrains ω close to the value of cosmological constant of ω does not indicate whether ω changes with time or not. So, theoretically, one could consider ω as a function of cosmic time, such as inflationary cosmology (see [28–32] for review). Scalar fields evolve in particle physics quite naturally. Till date, a large variety of scalar field inflationary models are discussed. This theory is active area in literature nowadays (see [20]). The scalar field which lightly interacts with gravity is called "quintessence." Quintessence fields are

first-hand choice because this field can lessen fine tuning problem of cosmological constant to some extent. Needless to say, some common drawbacks for quintessence also exist. Observations point that, at current epoch energy, density of scalar field and matter energy density are comparable. But we know that they evolve from different initial conditions. This discrepancy (known as "coincidence problem") arises for any scalar field dark energy; quintessence too suffers from this problem [33]. Of course, there is resolution of this problem; it is called "tracking solution" [34]. In the tracking regime, field value should be of the order of Planck mass. Anyway, a general setback is that we always need to seek for such potentials (see [35] for related discussion). EoS parameter ω of quintessence satisfies $-1 \leq \omega \leq 1$. Some current data indicates that ω lies in small neighbourhood of $\omega = -1$. Hence, it is technically feasible to relax ω to go down the line $\omega < -1$ [36]. There exists another scalar field with negative kinetic energy term, which can describe late acceleration. This is named as phantom field, which has EoS $\omega < -1$ (see details in [20, 37]). Phantom field energy density increases with time. As a result, Hubble factor and curvature diverges in finite time causing "Big Rip" singularity (see [38–40]). By the way, some specific choice of potential can avoid this flaw. Present data perhaps favours a dark energy model with $\omega > -1$ of recent past to $\omega < -1$ at present time [41]. The line $\omega = -1$ is known as "phantom" divide. Evidently, neither quintessence nor phantom field alone can cross the phantom divide. In this direction, a first-hand choice is to combine both quintessence and phantom field. This is known in the literature as "quintom" (i.e., hybrid of quintessence and phantom) [41]. This can serve the purpose but still has some fallacy. A single canonical complex field is quite natural and useful (like "spintessence" model [42, 43]). However, canonical complex scalar fields suffer a serious setback, namely, the formation of "Q-ball" (a kind of stable nontopological soliton) [42, 43].

To overcome various difficulties with above-mentioned models, Wei et al. in their paper [44, 45] introduced a non-canonical complex scalar field which plays the role of quintom [45–47]. They name this unique model as "hessence." However, hessence is unlike other canonical complex scalar fields which suffer from the formation of Q-ball. Second kind of theory modifies the classical general relativity (GR) by higher degree curvature terms (namely, $f(R)$ theory) [48–50] or by replacing symmetric Levi-Civita connection in GR theory by antisymmetric Weitzenböck connection. In other words, torsion is taken for gravitational interaction instead of curvature. The resulting theory [51–53] (called "teleparallel" gravity) was considered initially by Einstein to unify gravity with electromagnetism in non-Riemannian Weitzenböck manifold. Later, further modification was done to obtain $f(T)$ gravity as in the same vein of $f(R)$ gravity theory [54]. Although the EoS of "cosmological constant" (ΛCDM model) is well within the various dataset, till now not a single observation can detect DE or DM, and search for possible alternative is on the way [55]. In this regard, alternate gravity theory (like $f(T)$) is really worth discussing. The work in [56] is a nice account in establishing matter stability of $f(T)$ theory in weak field limit in contrast to $f(R)$ theory. It is shown that any choice of $f(T)$ can be used. Other reasons for the theoretical advantage for their choice are discussed in the next section.

We, in this work, have chosen hessence in $f(T)$ gravity. Since the system is complex, we have preferred a dynamical analysis. As we have mentioned previously, hessence field and $f(T)$ theory both are promising candidates to explain present accelerated phase. So, we merged them to find if they can highlight present acceleration more accurately with current dataset. A mixed dynamical system with tachyon, quintessence, and phantom in $f(T)$ theory is considered in [57]. Dynamical systems with quintom also exist in literature (see [58, 59] for review). The dynamical system analysis for normal scalar field model in $f(T)$ gravity has been discussed in [60]. But, to the best of our knowledge, hessence in $f(T)$ gravity has not been considered before.

We arrange the paper in the following manner. Short sketch of $f(T)$ theory is presented in Section 2. Hessence field in $f(T)$ gravity is introduced to form dynamical system in Section 3. Section 4 is devoted to dynamical system analysing and the stability of the system for hessence dark energy model. The significance of our result is discussed in Section 5 in light of recent data. We conclude the paper with relevant remarks in Section 6. We use normalized units as $8\pi G = \hbar = c = 1$ in this paper.

2. A Brief Outline of $f(T)$ Gravity: Some Basic Equations

In teleparallelism [54, 61, 62], e_A^μ are called the orthonormal tetrad components ($A = 0, 1, 2, 3$). The index A is used for each point x^μ for a tangent space of the manifold; hence each e_A^μ represents a tangent vector to the manifold (i.e., the so-called vierbein). Also the inverse of the vierbein is obtained from the relation $e_A^\mu e_\nu^A = \delta_\nu^\mu$. The metric tensor is given as $g_{\mu\nu} = \eta_{AB} e_\mu^A e_\nu^A$ ($\mu, \nu = 0, 1, 2, 3$); μ, ν are coordinate indices on the manifold (here, $\eta_{AB} = \mathrm{diag}(1, -1, -1, -1)$). Recently, to explain the acceleration, the teleparallel torsion (T) in Lagrangian density has been modified from linear torsion to some differentiable function of T [63, 64] (i.e., $f(T)$) like $f(R)$ theory mentioned earlier. In this new setup of gravity, the field equation is of second order unlike $f(R)$ (which is of fourth order). In $f(T)$ theory of gravitation, corresponding action reads

$$\mathcal{A} = \frac{1}{2\kappa^2} \int d^4x \left[\sqrt{-g}\,(T + f(T)) + \mathcal{L}_m\right], \tag{1}$$

where T is the torsion scalar, $f(T)$ is some differentiable function of torsion T, $\mathcal{L}_m$ is the matter Lagrangian, $\sqrt{-g} = \det(e_\mu^A)$, and $\kappa^2 = 8\pi G$. The torsion scalar T mentioned above is defined as

$$T = S_\rho{}^{\mu\nu} T^\rho{}_{\mu\nu} \tag{2}$$

with the components of torsion tensor $T^\rho{}_{\mu\nu}$ of (2) given by

$$T^\rho{}_{\mu\nu} = \Gamma^{W\lambda}{}_{\nu\mu} - \Gamma^{W\lambda}{}_{\mu\nu} = e_A^\lambda \left(\partial_\mu e_\nu^A - \partial_\nu e_\mu^A\right), \tag{3}$$

where $\Gamma^{W\lambda}{}_{\nu\mu} = e^{\lambda}_{A}\partial_{\mu}e^{A}_{\nu}$ is the Weitzenböck connection. Here, the superpotential $S_{\rho}{}^{\mu\nu}$ (2) is defined as follows:

$$S_{\rho}{}^{\mu\nu} = \frac{1}{2}\left(K^{\mu\nu}{}_{\rho} + \delta^{\mu}_{\rho}T^{\theta\nu}{}_{\theta} - \delta^{\nu}_{\rho}T^{\theta\mu}{}_{\theta}\right),$$
$$K^{\mu\nu}{}_{\rho} = (-)\frac{1}{2}\left(T^{\mu\nu}{}_{\rho} - T^{\nu\mu}{}_{\rho} - T_{\rho}{}^{\mu\nu}\right). \quad (4)$$

$K^{\mu\nu}{}_{\rho}$ is called contortion tensor. The contortion tensor measures the difference between symmetric Levi-Civita connection and antisymmetric Weitzenböck connection. It is easy to check that the equation of motion reduces to Einstein gravity if $f(T) = 0$. Actually this is the correspondence between teleparallel gravity and Einsteinian theory [53]. It is noticed that $f(T)$ theory can address early acceleration and late evolution of universe depending on the choice of $f(T)$. For example, power law or exponential form cannot overcome phantom divide [65], but some other choices of $f(T)$ [66] can cross phantom divide. The reconstruction of $f(T)$ model [67, 68], various cosmological [69, 70] and thermodynamical [71] analysis, has been reported. It is so interesting to note that linear $f(T)$ model (i.e., when dF/dT = constant) behaves as cosmological constant. Anyway, a preferable choice of $f(T)$ is such that it reduces to general relativity (GR) when redshift is large in tune with primordial nucleosynthesis and cosmic microwave data at early times (i.e., $f/T \to 0$ for $a \ll 1$). Moreover, in future, it should give de-Sitter-like state. One such choice is given in power form as in [72]; namely,

$$f(T) = \beta(-T)^{n}, \quad (5)$$

with β being a constant. In particular, $n = 1/2$ gives same expanding model as the theory referred to in [72, 73]. Current data needs the bound "$n \ll 1$" to permit $f(T)$ as an alternate gravity theory. The effective DE equation of state varies from $\omega = -1 + n$ of past to $\omega = -1$ in future.

Throughout the work, we assume flat, homogeneous, isotropic Friedmann-Lemaître-Robertson-Walker (FLRW) metric,

$$ds^{2} = dt^{2} - a^{2}(t)\sum_{i=1}^{3}\left(dx^{i}\right)^{2}, \quad (6)$$

which arises from the vierbein $e^{A}_{\mu} = \mathrm{diag}(1, a(t), a(t), a(t))$. Here, $a(t)$ is the scale factor as a function of cosmic time t. Using (3) and (4), one gets

$$T = S^{\rho\mu\nu}T_{\rho\mu\nu} = -6H^{2}, \quad (7)$$

where $H = \dot{a}(t)/a(t)$ is the Hubble factor (from here and in the rest of the paper "overdot" will mean the derivative operator d/dt).

3. Hessence Dark Energy in $f(T)$ Gravity Theory: Formation of Dynamical Equations

Here, we consider a noncanonical complex scalar field:

$$\Phi = \phi_{1} + i\phi_{2}, \quad (8)$$

where $i = \sqrt{-1}$ with Lagrangian density:

$$\mathscr{L}_{\mathrm{DE}} = \frac{1}{4}\left[\left(\partial_{\mu}\Phi\right)^{2} + \left(\partial_{\mu}\Phi^{*}\right)^{2}\right] - V(\Phi, \Phi^{*}). \quad (9)$$

Clearly the Lagrangian density is identical to the Lagrangian given by two real scalar fields, which looks like

$$\mathscr{L}_{\mathrm{DE}} = \frac{1}{2}\left(\partial_{\mu}\phi_{1}\right)^{2} - \frac{1}{2}\left(\partial_{\mu}\phi_{2}\right)^{2} - V(\phi_{1}, \phi_{2}), \quad (10)$$

where ϕ_1 and ϕ_2 are quintessence and phantom fields, respectively. It is noteworthy that the Lagrangian in (9) consists of one field instead of two independent fields as in (10) of [41]. It also differs from canonical complex scalar field (like "spintessence" in [42, 43]) which has the Lagrangian

$$\mathscr{L}_{\mathrm{DE}} = \frac{1}{2}\left(\partial_{\mu}\Psi^{*}\right)\left(\partial_{\mu}\Psi\right) - V(|\Psi|), \quad (11)$$

where $|\Psi|$ denotes the absolute value of Ψ; that is, $|\Psi|^{2} = \Psi^{*}\Psi$. However, hessence is unlike canonical complex scalar fields which suffer from the formation of "Q-ball" (a kind of stable nontopological soliton). Following Wei et al. as in [44, 45], the energy density ρ_h and pressure p_h of hessence field can be written as

$$\rho_{h} = \frac{1}{2}\left(\dot{\phi}^{2} - \frac{Q^{2}}{a^{6}\phi^{2}}\right) + V(\phi), \quad (12)$$

$$p_{h} = \frac{1}{2}\left(\dot{\phi}^{2} - \frac{Q^{2}}{a^{6}\phi^{2}}\right) - V(\phi), \quad (13)$$

where Q is a constant and denotes the total induced charge in the physical volume (refer to [44, 45]). In this paper, we will consider interaction of hessence field and matter. The matter is perfect fluid with barotropic equation of state:

$$p_{m} = w_{m}\rho_{m} \equiv (\gamma - 1)\rho_{m}, \quad (14)$$

where γ is the barotropic index satisfying $0 < \gamma \leq 2$. Also p_m and ρ_m, respectively, denote the pressure and energy density of matter. In particular $\gamma = 1$ and $\gamma = 4/3$ indicate dust matter and radiation, respectively. We suppose that hessence and background fluid interact through a term C. This term C indicates energy transfer between dark energy and dark matter. Positive C is needed to solve coincidence problem, since positive magnitude of C indicates energy transfer from dark energy to dark matter. Also 2^{ND} law of thermodynamics is also valid with this choice. An interesting work to settle this problem is reviewed in [74]. A rigorous dynamical analysis is done there. Similar approach exists for quintom model, too. Various choices of this interaction term C are used in the literature. Here, in view of dimensional requirement of energy conservation equation and to make the dynamical system simple, we have taken $C = \delta\dot{\phi}\rho_{m}$, where δ is a real constant of small magnitude, which may be chosen as positive or negative at will, such that C remains positive. Also, $\dot{\phi}$ may be positive or negative according to the hessence field ϕ. So we have

$$\dot{\rho}_{h} + 3H(\rho_{h} + p_{h}) = -C, \quad (15)$$

$$\dot{\rho}_{m} + 3H(\rho_{m} + p_{m}) = C, \quad (16)$$

preserving the total energy conservation equation:

$$\dot{\rho}_{\text{total}} + 3H\left(\rho_{\text{total}} + p_{\text{total}}\right) = 0. \tag{17}$$

The modified field equations in $f(T)$ gravity are

$$H^2 = \frac{1}{(2f_T + 1)}\left[\frac{1}{3}\left(\rho_h + \rho_m\right) - \frac{f}{6}\right], \tag{18}$$

$$\dot{H} = \left(-\frac{1}{2}\right)\left[\frac{\rho_h + p_h + \rho_m}{1 + f_T + 2Tf_T}\right]. \tag{19}$$

In view of (12) and (15), we have

$$\ddot{\phi} + 3H\dot{\phi} + \frac{Q^2}{a^6\phi^2} + V' = -\delta\rho_m. \tag{20}$$

Here, "$'$" means "$d/d\phi$." Similarly, (14) and (16) give

$$\dot{\rho}_m + 3H\gamma\rho_m = \delta\dot{\phi}\rho_m. \tag{21}$$

Now, we introduce five auxiliary variables:

$$\begin{aligned} x &= \frac{\dot{\phi}}{\sqrt{6}H}, \\ y &= \frac{\sqrt{V}}{\sqrt{3}H}, \\ u &= \frac{\sqrt{6}}{\phi}, \\ v &= \frac{Q}{\sqrt{6}H\sqrt{a^3\phi}}, \\ \Omega_m &= \frac{\rho_m}{3H^2}. \end{aligned} \tag{22}$$

We form the following autonomous system after some manipulation:

$$\begin{aligned} \frac{dx}{dN} &= -3x - uv^2 - \lambda\sqrt{\frac{3}{2}}y^2 - \delta\sqrt{\frac{3}{2}}\Omega_m \\ &\quad + \frac{3x}{2}\left(2x^2 - 2v^2 + \Omega_m\right), \\ \frac{dy}{dN} &= \lambda\sqrt{\frac{3}{2}}xy + \frac{3}{2}y\left(2x^2 - 2v^2 + \Omega_m\right), \\ \frac{du}{dN} &= -xu^2, \\ \frac{dv}{dN} &= -xuv - 3v + \frac{3}{2}v\left(2x^2 - 2v^2 + \Omega_m\right), \\ \frac{d\Omega_m}{dN} &= \Omega_m\left(-3\gamma - \delta\sqrt{6}x + 3\left(2x^2 - 2v^2 + \Omega_m\right)\right). \end{aligned} \tag{23}$$

In above calculations, $N = \int(\dot{a}/a)dt = \ln a$ denotes the "e-folding" number. We have chosen N as independent variable. We have taken $f(T) = \beta\sqrt{-T}$ for above derivation of autonomous system. Also, we have chosen exponential form of potential, that is, $V'/V = \lambda$ (where λ is a real constant), for simplicity of the autonomous system. This kind of choice is standard in literature with coupled real scalar field [75] and complex field (like hessence in loop quantum cosmology) in [59]. The work in [60] dealing with quintessence, matter in $f(T)$ theory, is also done with exponential potential. But, to our knowledge, hessence, matter in $f(T)$ theory, has not been considered before. In view of (22), the Friedmann equation (18) reduces as

$$x^2 + y^2 - v^2 + \Omega_m = 1. \tag{24}$$

The Raychaudhuri equation becomes

$$-\frac{\dot{H}}{H^2} = \frac{3}{2}\left(2x^2 - 2v^2 + \Omega_m\right). \tag{25}$$

The density parameters of hessence (Ω_h) dark energy and background matter (Ω_m) are obtained in the following forms:

$$\begin{aligned} \Omega_h &= \frac{\rho_h}{3H^2} = x^2 + y^2 - v^2, \\ \Omega_m &= \frac{\rho_m}{3H^2} = 1 - \left(x^2 + y^2 - v^2\right). \end{aligned} \tag{26}$$

The EoS of hessence ω_h dark energy and total EoS of the system ω_{total} are calculated in the following forms:

$$\begin{aligned} \omega_h &= \frac{p_h}{\rho_h} = \frac{x^2 - y^2 - v^2}{x^2 + y^2 - v^2}, \\ \omega_{\text{total}} &= \frac{p_h + p_m}{\rho_h + \rho_m} = x^2 - y^2 - v^2 + (\gamma - 1)\Omega_m. \end{aligned} \tag{27}$$

Also, the deceleration parameter q can be expressed as

$$q = -1 - \frac{\dot{H}}{H^2} = -1 + \frac{3}{2}\left(2x^2 - 2v^2 + \Omega_m\right). \tag{28}$$

4. Fixed Points and Stability Analysis of the Autonomous System

4.1. Fixed Points with Exponential Potential. We have made the choice of exponential form of potential, that is, $V'/V = \lambda$ (where λ is a real constant). The fixed points P_i, the coordinates of P_i, that is, (x_c, y_c, u_c, v_c, Ω_{mc}), are given in Table 1 with relevant parameters and existence condition(s).

From Table 1, we note the following.

Case 1. Fixed points $P_1, P_2 = (\pm 1, 0, 0, 0, 0)$ always exist with the physical parameters $\Omega_m = 0$, $\omega_h = 1$, $\omega_{\text{total}} = 1$, $\Omega_h = 1$, and $q = 2$.

Case 2. Fixed point $P_{3\pm} = (\pm 1 \text{ or } (6 - 3\gamma)/\delta\sqrt{6}, 0, 0, 0, 0)$ exists under the condition that $(6 - 3\gamma)/\delta\sqrt{6} = \pm 1$ with the physical parameters $\Omega_m = 0$, $\omega_h = 1$, $\omega_{\text{total}} = 1$, $\Omega_h = 1$, and $q = 2$, that is, same as P_1 and P_2.

Case 3. Fixed point $P_4 = (-\sqrt{(2/3)}\delta, 0, 0, 0, (6 - 3\gamma + 2\delta^2)/3)$ exists under the condition that $2\delta^2/3 + (6 - 3\gamma + 2\delta^2)/3 = 1$

Table 1: Fixed points of the autonomous system of equations (23) and various physical parameters with existence conditions. Here $A = -\sqrt{(3/2)}(\gamma/(\delta+\lambda))$ and $B = (6+\lambda\sqrt{6}A - 6A^2)/9$.

P_i	$x_c, y_c, u_c, v_c, \Omega_{mc}$	Ω_m	ω_h	ω_{total}	Ω_h	q	Existence condition(s)
P_1	1, 0, 0, 0, 0	0	1	1	1	2	Always
P_2	–1, 0, 0, 0, 0	0	1	1	1	2	Always
$P_{3\pm}$	± 1 or $\frac{6-3\gamma}{\delta\sqrt{6}}$, 0, 0, 0, 0	0	1	1	1	2	$\frac{6-3\gamma}{\delta\sqrt{6}} = \pm 1$
P_4	$-\sqrt{\frac{2}{3}}\delta$, 0, 0, 0, $\frac{6-3\gamma+2\delta^2}{3}$	$\frac{6-3\gamma+2\delta^2}{3}$	1	$\gamma(1-\frac{2\delta^2}{3})+\frac{4\delta^2}{3}-1$	$\frac{2\delta^2}{3}$	$\frac{1}{2}+\delta^2$	$\frac{2\delta^2}{3}+\frac{6-3\gamma+2\delta^2}{3} = 1$
P_5	$x = \frac{6-3\gamma}{\delta\sqrt{6}}$, 0, 0, $\sqrt{x^2-1}$, 0	0	1	1	1	2	$6\delta^2 \le (6-3\gamma)^2$
P_6	$x = \frac{6-3\gamma}{\delta\sqrt{6}}$, 0, 0, $-\sqrt{x^2-1}$, 0	0	1	1	1	2	$6\delta^2 \le (6-3\gamma)^2$
P_7	0, 1, any value, 0, 0	0	–1	–1	1	–1	$\gamma = 0$
P_8	0, 1, any value, 0, 0	0	–1	–1	1	–1	$\gamma = 0$
P_9	$-\frac{\lambda}{\sqrt{6}}$, $\sqrt{1-\frac{\lambda^2}{6}}$, 0, 0, 0	0	$-1+\frac{\lambda^2}{3}$	$-1+\frac{\lambda^2}{3}$	1	$-1+\frac{\lambda^2}{2}$	$\lambda^2 \le 6$
P_{10}	$-\frac{\lambda}{\sqrt{6}}$, $-\sqrt{1-\frac{\lambda^2}{6}}$, 0, 0, 0	0	$-1+\frac{\lambda^2}{3}$	$-1+\frac{\lambda^2}{3}$	1	$-1+\frac{\lambda^2}{2}$	$\lambda^2 \le 6$
P_{11}	A, $\sqrt{1-A^2-B^2}$, 0, 0, B	B	$\frac{-1+2A^2+B^2}{1-B}$	$-1+A^2+B^2+(\gamma-2)B$	$1-B$	$-1+\frac{3}{2}B+3B^2$	$\delta+\lambda \ne 0$
P_{12}	A, $-\sqrt{1-A^2-B^2}$, 0, 0, B	B	$\frac{-1+2A^2+B^2}{1-B}$	$-1+A^2+B^2+(\gamma-2)B$	$1-B$	$-1+\frac{3}{2}B+3B^2$	$\delta+\lambda \ne 0$
P_{13}	$-\frac{\sqrt{6}}{\lambda}$, 0, 0, $\sqrt{\frac{6}{\lambda^2}-1}$, 0	0	1	1	1	2	$\lambda^2 \le 6$
P_{14}	$-\frac{\sqrt{6}}{\lambda}$, 0, 0, $-\sqrt{\frac{6}{\lambda^2}-1}$, 0	0	1	1	1	2	$\lambda^2 \le 6$
P_{15}	$x = -\frac{6}{\lambda} = \frac{6-3\gamma}{\delta\sqrt{6}}$, 0, 0, $\sqrt{x^2-1}$, 0	0	1	1	1	2	$-\frac{6}{\lambda} = \frac{6-3\gamma}{\delta\sqrt{6}}$ and $\lambda \ne 2\delta$
P_{16}	$x = -\frac{6}{\lambda} = \frac{6-3\gamma}{\delta\sqrt{6}}$, 0, 0, $-\sqrt{x^2-1}$, 0	0	1	1	1	2	$-\frac{6}{\lambda} = \frac{6-3\gamma}{\delta\sqrt{6}}$ and $\lambda \ne 2\delta$

with physical parameters $\Omega_m = (6 - 3\gamma + 2\delta^2)/3$, $\omega_h = 1$, $\omega_{\text{total}} = -1+\gamma(1-2\delta^2/3)+4\delta^2/3$, $\Omega_h = 2\delta^2/3$, and $q = 1/2+\delta^2$.

Case 4. Fixed points $P_5, P_6 = (x = (6 - 3\gamma)/\delta\sqrt{6}, 0, 0, \pm\sqrt{x^2 - 1}, 0)$ exist under the condition that $6\delta^2 \leq (6 - 3\gamma)^2$ with physical parameters $\Omega_m = 0$, $\omega_h = 1$, $\omega_{\text{total}} = 1$, $\Omega_h = 1$, and $q = 2$.

Case 5. Fixed points $P_7, P_8 = (0, 1, \text{any value}, 0, 0)$ exist under the condition that $\gamma = 0$ with physical parameters $\Omega_m = 0$, $\omega_h = -1$, $\omega_{\text{total}} = -1$, $\Omega_h = 1$, and $q = -1$.

Case 6. Fixed points $P_9, P_{10} = (-\lambda/\sqrt{6}, \pm\sqrt{1 - \lambda^2/6}, 0, 0, 0)$ exist under the condition that $\lambda^2 \leq 6$ with physical parameters $\Omega_m = 0$, $\omega_h = -1 + \lambda^2/3$, $\omega_{\text{total}} = -1 + \lambda^2/3$, $\Omega_h = 1$, and $q = -1 + \lambda^2/2$.

Case 7. Fixed points $P_{11}, P_{12} = (A, \pm\sqrt{1 - A^2 - B^2}, 0, 0, B)$ exist under the condition that $\delta + \lambda \neq 0$ with physical parameters $\Omega_m = B$, $\omega_h = (-1 + 2A^2 + B^2)/(1 - B)$, $\omega_{\text{total}} = -1 + A^2 + B^2 + (\gamma - 2)B$, $\Omega_h = 1 - B$, and $q = -1 + (3/2)B + 3B^2$.

Case 8. Fixed points $P_{13}, P_{14} = (-\sqrt{6}/\lambda, 0, 0, \pm\sqrt{6/\lambda^2 - 1}, 0)$ exist under the condition that $\lambda^2 \leq 6$ with physical parameters $\Omega_m = 0$, $\omega_h = 1$, $\omega_{\text{total}} = 1$, $\Omega_h = 1$, and $q = 2$.

Case 9. Fixed points $P_{15}, P_{16} = (x = -6/\lambda = (6 - 3\gamma)/\delta\sqrt{6}, 0, 0, \pm\sqrt{x^2 - 1}, 0)$ exist under the condition that $-6/\lambda = (6 - 3\gamma)/\delta\sqrt{6}$ and $\lambda \neq 2\delta$ with physical parameters $\Omega_m = 0$, $\omega_h = 1$, $\omega_{\text{total}} = 1$, $\Omega_h = 1$, and $q = 2$.

4.2. Stability of the Fixed Points. Dynamical analysis is a powerful technique to study cosmological evolution, where exact solution could not be found due to complicated system. This can be done without any information of specific initial conditions. The dynamical systems mostly encountered in cosmological system are nonlinear systems of differential equations (DE). Here the dynamical system is also nonlinear. Very few works in literature are devoted to analysing nonlinear dynamical systems. But we used the methods developed till now [76]. Also we devised some method (as in the plotting of the dynamical evolution and use of normally hyperbolic fixed points). We now analyse stability of the fixed points. In this regard, we find the eigenvalues of the linear perturbation matrix of the dynamical system (23). Due to the Friedmann equation (24), we have four independent perturbed equations. The eigenvalues of the 4×4 linear perturbation matrix corresponding to each fixed point P_i are given in Table 2. Before further discussion, we state some basics from nonlinear system of differential equation (DE) [76]. If the real part of each eigenvalue is nonzero, then the fixed point is called hyperbolic fixed point (otherwise, it is called nonhyperbolic). Let us write a nonlinear system of DE in R^n *(the n-dimensional Euclidean plane) as*

$$\dot{x} = f(x), \tag{29}$$

where $f : E \to R^n$ is derivable and E is an open set in R. For nonlinear system, the DE cannot be written in matrix form as done in linear system. Near hyperbolic fixed point, a nonlinear dynamical system could be linearized and stability of the fixed point is found by Hartman-Grobman theorem. As we can see from the following, let x_c be a fixed point and let $\zeta(t)$ be the perturbation from x_c; that is, $\zeta(t) = x - x_c$; that is, $x = x_c + \zeta(t)$. We find the time evolution of $\zeta(t)$ for (29) as

$$\dot{\zeta} = \frac{d}{dt}(x - x_c) = \dot{x} = f(x) = f(x_c + \zeta). \tag{30}$$

Since f is assumed to be derivable, we use the Taylor expansion of f to get

$$f(x_c + \zeta) = f(x_c) + \zeta Df(x_c) + \cdots. \tag{31}$$

$Df(x) = \partial f_i/\partial x_j$, $i, j = 1, 2, \ldots, n$; as ζ is very small, higher order terms are neglected above. As $f(x_c) = 0$, (30) reduces to

$$\dot{\zeta} = \zeta Df(x_c). \tag{32}$$

This is called the linearization of the DE near a fixed point. Stability of the fixed point x_c is inferred from the sign of eigenvalues of Jacobian matrix $Df(x_c)$. If the fixed point is hyperbolic, then stability is concluded from Hartman-Grobman theorem, which states the following.

Theorem (Hartman-Grobman). Given the nonlinear DE (29) in R^n, where f is derivable with flow ϕ_t, if x_c is a hyperbolic fixed point, then there exists a neighbourhood N of x_c, on which ϕ_t is homeomorphic to the flow of linearization of the DE near x_c.

But for nonhyperbolic fixed point this cannot be done and the study of stability becomes hard due to lack of theoretical setup. If at least one eigenvalue corresponding to the fixed point is zero, then it is termed as nonhyperbolic. For this case, we cannot find out stability near the fixed point. Consequently, we have to resort to other techniques like numerical solution of the system near fixed point and to study asymptotic behaviour with the help of plot of the solution, as is done in this work (details are described later). However, we can find the dimension of stable manifold (if exists) with the help of centre manifold theorem. There is a separate class of important nonhyperbolic fixed points known as normally hyperbolic fixed points, which are rarely considered in literature (see [77]). As some fixed points encountered in our work are of this kind, we state the basics here. We are also interested in nonisolated normally hyperbolic fixed points of a given DE (e.g., a curve of fixed points; such a set is called equilibrium set). If an equilibrium set has only one zero eigenvalue at each point and all other eigenvalues have nonzero real part, then the equilibrium set is called normally hyperbolic. The stability of normally hyperbolic fixed point is deduced from invariant manifold theorem, which states the following.

Theorem (Invariant Manifold). Let $x = x_c$ be a fixed point of the DE $\dot{x} = f(x)$ on R^n and let E^s, E^u, and E^c denote the stable, unstable, and centre subspaces of the linearization of the DE at x_c. Then there exist a stable manifold W^s

Table 2: Eigenvalues of the fixed points of the autonomous system of equations (23) and the nature of stability (if any), where $D = -12 + 24a^2 + 12b^2 + 2\sqrt{6}a\delta + \sqrt{6}a\lambda$ and $\Delta = -144a^2 + 144a^4 + 144a^2b^2 + 36b^4 + 48\sqrt{6}a\delta - 48\sqrt{6}a^3\delta - 72\sqrt{6}ab^2\delta + 24a^2\delta^2 - 72\sqrt{6}a\lambda + 72\sqrt{6}a^3\lambda + 84\sqrt{6}ab^2\lambda + 48\delta\lambda - 72a^2\delta\lambda - 48b^2\delta\lambda - 48\lambda^2 + 54a^2\lambda^2 + 48b^2\lambda^2$.

P_i	Eigenvalues	Nature of stability (if exists†)
P_1	$0, 0, 3 + \delta\sqrt{6}, 3 + \sqrt{\frac{3}{2}}\lambda$	2D stable manifold
P_2	$0, 0, 3 - \delta\sqrt{6}, 3 - \sqrt{\frac{3}{2}}\lambda$	2D stable manifold
$P_{3\pm}$	$0, 0, 3 \pm \delta\sqrt{6}, 3 \pm \sqrt{\frac{3}{2}}\lambda$	2D stable manifold
P_4	$0, -\frac{3}{2} + \delta^2, -\frac{3}{2} + \delta^2, \frac{3}{2} + \delta^2 - \delta\lambda$	3D stable manifold
P_5	$0, 0, 3 + \sqrt{6}x\delta, 3 + \sqrt{\frac{3}{2}}x\lambda$	2D stable manifold
P_6	$0, 0, 3 + \sqrt{6}x\delta, 3 + \sqrt{\frac{3}{2}}x\lambda$	2D stable manifold
P_7	$-3, 0, -3 - \sqrt{3(\delta\lambda - \lambda^2)}, -3 + \sqrt{3(\delta\lambda - \lambda^2)}$	stable
P_8	$-3, 0, -3 - \sqrt{3(\delta\lambda - \lambda^2)}, -3 + \sqrt{3(\delta\lambda - \lambda^2)}$	stable
P_9	$0, -3 + \frac{\lambda^2}{2}, -3 + \frac{\lambda^2}{2}, -3 - \delta\lambda + \lambda^2$	3D stable manifold
P_{10}	$0, -3 + \frac{\lambda^2}{2}, -3 + \frac{\lambda^2}{2}, -3 - \delta\lambda + \lambda^2$	3D stable manifold
P_{11}	$0, -3 + 3a^2 + 3\frac{b^2}{2}, \frac{1}{4}(D - \sqrt{\Delta}), \frac{1}{4}(D + \sqrt{\Delta})$	3D stable manifold
P_{12}	$0, -3 + 3a^2 + 3\frac{b^2}{2}, \frac{1}{4}(D - \sqrt{\Delta}), \frac{1}{4}(D + \sqrt{\Delta})$	3D stable manifold
P_{13}	$0, 0, 0, -3\frac{(2\delta\lambda - \lambda^2)}{\lambda^2}$	1D stable manifold
P_{14}	$0, 0, 0, -3\frac{(2\delta\lambda - \lambda^2)}{\lambda^2}$	1D stable manifold
P_{15}	$0, 0, 3 + \sqrt{6}x\delta, 3 + \sqrt{\frac{3}{2}}x\lambda$	2D stable manifold
P_{16}	$0, 0, 3 + \sqrt{6}x\delta, 3 + \sqrt{\frac{3}{2}}x\lambda$	2D stable manifold

†Nature of stability is discussed in detail.

tangent to E^s, an unstable manifold W^s tangent to E^u, and a centre manifold W^c tangent to E^c at x_c. In other words, the stability depends on the sign of remaining eigenvalues. If the sign of remaining eigenvalues is negative, then the fixed point is stable; otherwise it is unstable. Table 2 shows the eigenvalues corresponding to the fixed points given in Table 1 and existence for hyperbolic, nonhyperbolic, or normally hyperbolic fixed points with the nature of stability (if any).

We see from Table 2 that each fixed point P_i is nonhyperbolic, except P_7 and P_8 (which are normally hyperbolic). So we cannot use linear stability analysis. Hence, we have utilised the following scheme to infer the stability of nonhyperbolic fixed points. We find the numerical solutions of the system of differential equations (23). Then, we have investigated the variation of the dynamical variables x, y, u, v, Ω_m against e-folding N, which in turn gives the variation against time t

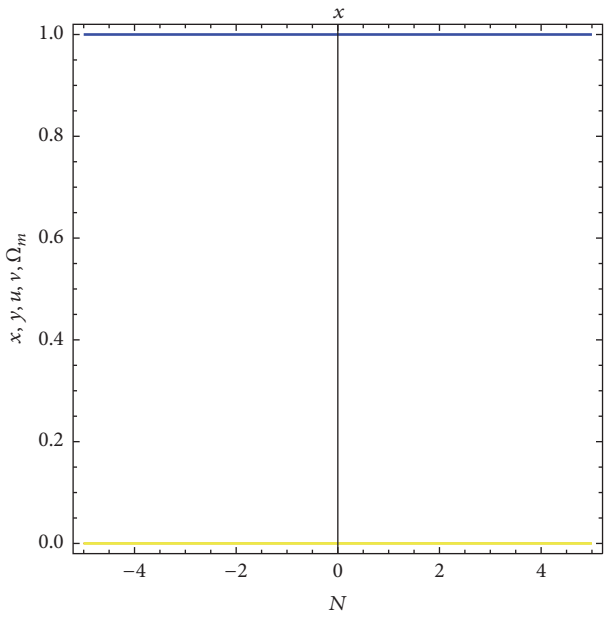

Figure 1: Plot of (1) variations of x (blue), y (green), u (orange), v (red), and Ω_m (yellow) versus N near P_1, for $\gamma = 1$, $\delta = 0.5$, and $\lambda = -0.5$. The position corresponding to $N = 0$ is the fixed point under consideration.

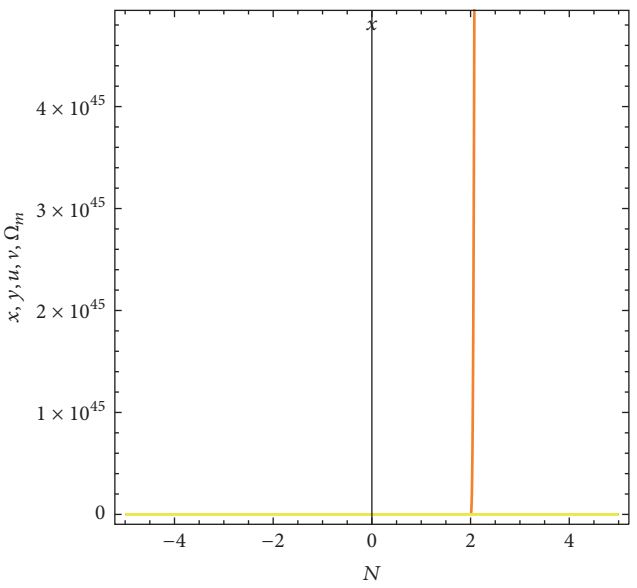

Figure 2: Plot of (2) variations of x (blue), y (green), u (orange), v (red), and Ω_m (yellow) versus N near P_2, for $\gamma = 1$, $\delta = 0.5$, and $\lambda = -0.5$. The position corresponding to $N = 0$ is the fixed point under consideration.

through graphs in the neighbourhood of each fixed point, and notice if the dynamical variables asymptotically converge to any of the fixed points. In that case, we can say that the fixed point is stable (otherwise, it is unstable). This method is used nowadays in absence of proper mathematical analysis of nonlinear dynamical system. But we must remember that the method is not full proof, since we have to consider the neighbourhood of N as large as possible (i.e., $|N| \to \infty$), because a small perturbation can lead to instability. The graphs corresponding to each fixed point are given and analysed below. We consider the fixed points one by one.

We note from Figure 1 that P_1 is not a stable fixed point. Similar is the case of P_2, as is evident from Figure 2. We note that if $\lambda \leq -\sqrt{6}$ and $\delta \leq -\sqrt{3/2}$ (or $\lambda \geq \sqrt{6}$ and $\delta \geq \sqrt{3/2}$) (equality should occur in one of them), then P_1 (or P_2) may admit 2-dimensional stable manifold corresponding to the two negative eigenvalues with EoS of hessence and total EoS being 1, and universe decelerates.

We note that $P_{3\pm}$ bears same feature as P_1 and P_2. So, none of P_1, P_2, and P_3 describes the current phase of universe. The points bear no physical significance.

If $\delta^2 \leq 3/2$ and $\delta^2 - \delta\lambda \leq -3/2$ (equality should occur in one of them), P_4 may admit 2-dimensional stable manifold corresponding to the two negative eigenvalues with EoS of hessence being 1 and total EoS is $-1 + \gamma(1 - 2\delta^2/3) + 4\delta^2/3$ and universe decelerates. Here, the plot in Figure 3 indicates that with a small increase of N the solution moves away from P_4. This is an unstable fixed point.

We note that, for P_5 and P_6, if $x\delta \leq -\sqrt{3/2}$ and $x\lambda \leq -\sqrt{6}$ (equality should occur in one of them), P_5 may admit 2-dimensional stable manifold corresponding to the two negative eigenvalues and P_6 too may admit 2-dimensional

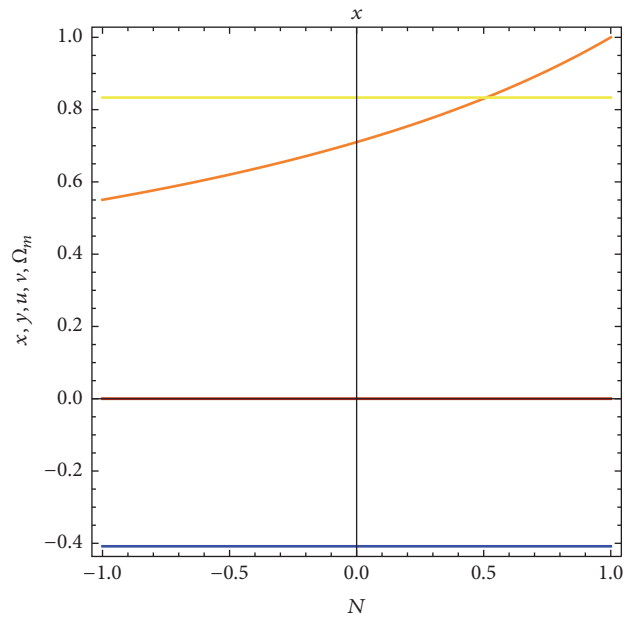

Figure 3: Plot of (3) variations of x (blue), y (green), u (orange), v (red), and Ω_m (yellow) versus N near P_4, for $\gamma = 4/3$, $\delta = 0.5$, and $\lambda = -0.5$. The position corresponding to $N = 0$ is the fixed point under consideration.

stable manifold corresponding to the two negative eigenvalues with EoS of hessence being 1 and total EoS is 1 and universe decelerates. Figure 4 indicates that the three of the variables (namely, x, v, and Ω_m) are moving away from P_5 and intruding in a neighbourhood of $N = 10$. This may denote the stable manifold corresponding to the negative eigenvalues. However, this point gives the decelerated phase

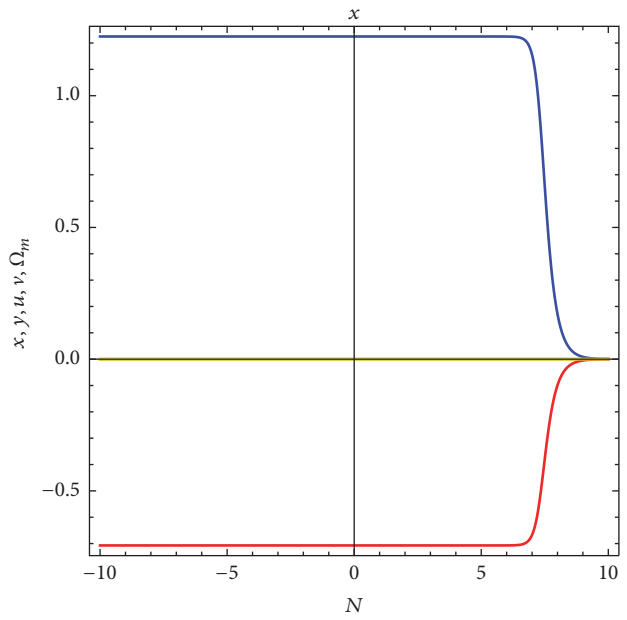

Figure 4: Plot of (4) variations of x (blue), y (green), u (orange), v (red), and Ω_m (yellow) versus N near P_5, for $\gamma = 1$, $\delta = 1$, and $\lambda = -0.5$. The position corresponding to $N = 0$ is the fixed point under consideration.

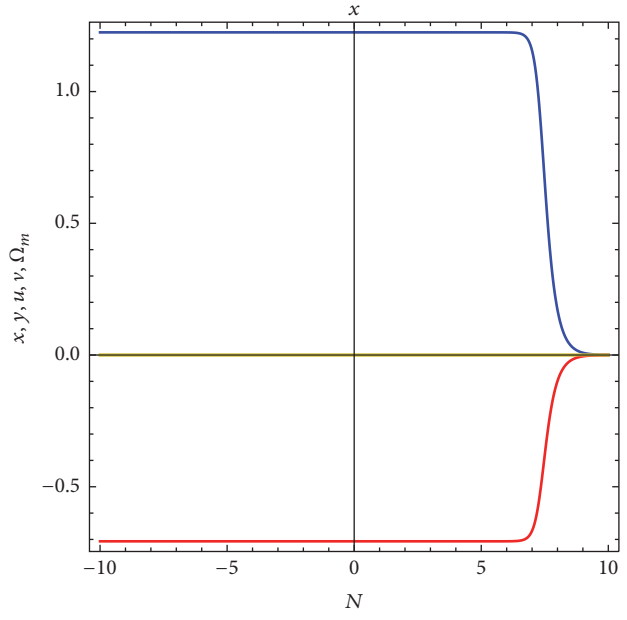

Figure 5: Plot of (5) variations of x (blue), y (green), u (orange), v (red), and Ω_m (yellow) versus N near P_6, for $\gamma = 1$, $\delta = 1$, and $\lambda = -0.5$. The position corresponding to $N = 0$ is the fixed point under consideration.

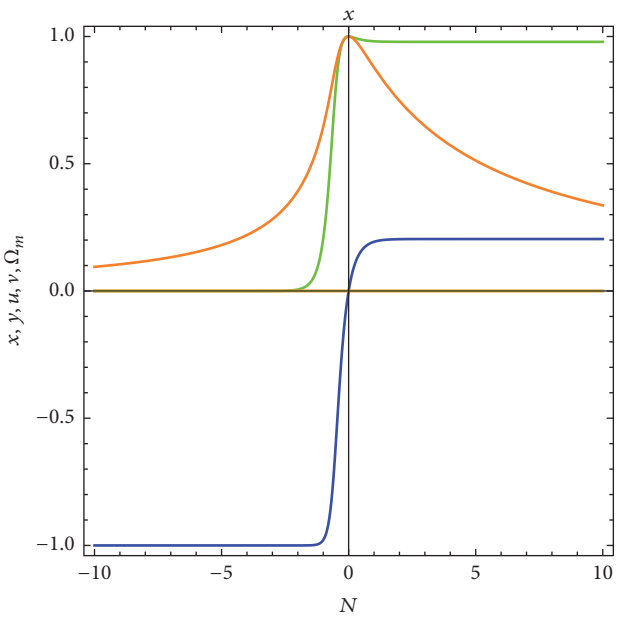

Figure 6: Plot of (6) variations of x (blue), y (green), u (orange), v (red), and Ω_m (yellow) versus N near P_7, for $\gamma = 0$, $\delta = 1$, and $\lambda = -0.5$. The position corresponding to $N = 0$ is the fixed point under consideration.

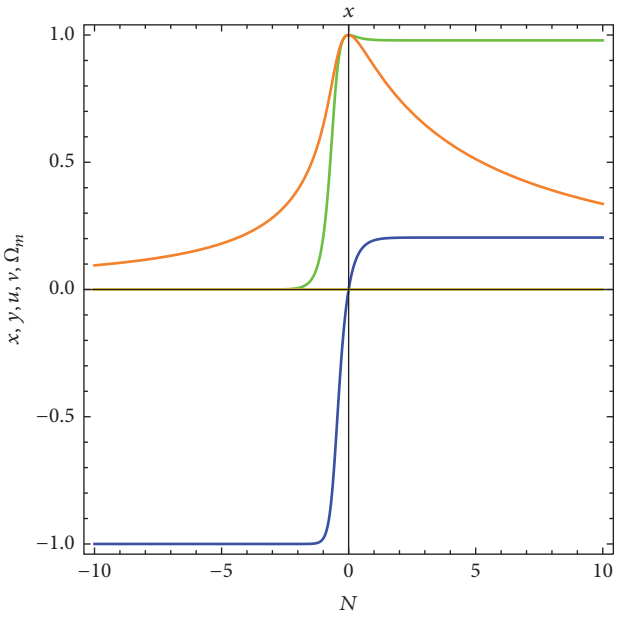

Figure 7: Plot of (7) variations of x (blue), y (green), u (orange), v (red), and Ω_m (yellow) versus N near P_8, for $\gamma = 0$, $\delta = 1$, and $\lambda = -0.5$. The position corresponding to $N = 0$ is the fixed point under consideration.

of the universe. Similar phenomena can be noted from Figure 5.

We note that if $\delta\lambda - \lambda^2 \leq 3$, both P_7 and P_8 are normally hyperbolic set of fixed points and as the rest three nonzero eigenvalues are negative, they are stable. The set of fixed points has EoS of hessence of -1 and total EoS is also -1 and universe accelerates like "cosmological constant." We note clearly from Figures 6 and 7 that all lines from negative and positive values of N (i.e., from past and future) are converging towards $N = 0$ (i.e., the set of fixed points).

We note that if $\lambda^2 \leq 6$ and $\lambda^2 - \delta\lambda \leq 3$ (equality should occur in one of them), P_9 and P_{10} may admit 3-dimensional

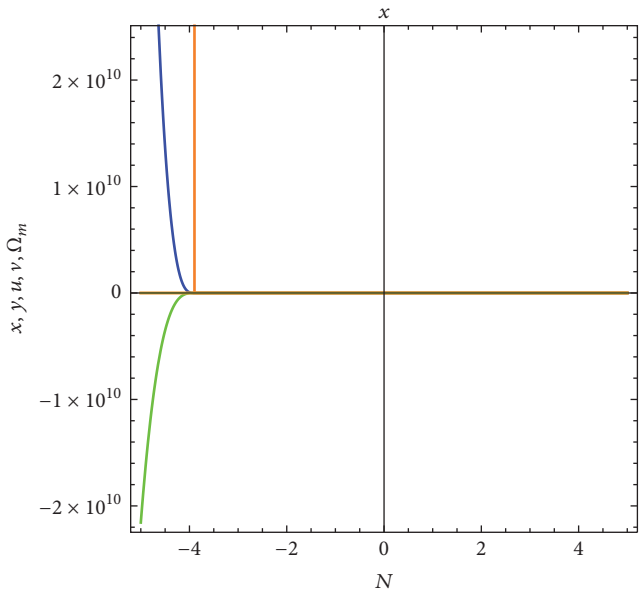

FIGURE 8: Plot of (8) variations of x (blue), y (green), u (orange), v (red), and Ω_m (yellow) versus N near P_9, for $\gamma = 1$, $\delta = 1$, and $\lambda = -0.5$. The position corresponding to $N = 0$ is the fixed point under consideration.

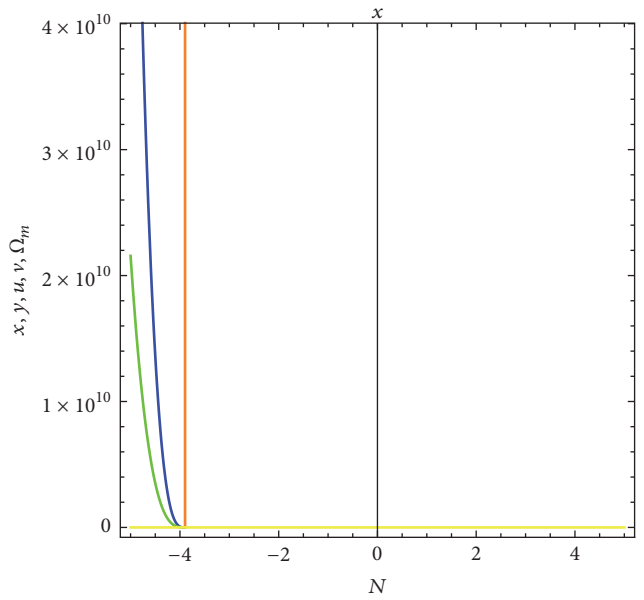

FIGURE 9: Plot of (9) variations of x (blue), y (green), u (orange), v (red), and Ω_m (yellow) versus N near P_{10}, for $\gamma = 1$, $\delta = 1$, and $\lambda = -0.5$. The position corresponding to $N = 0$ is the fixed point under consideration.

stable manifold corresponding to the negative eigenvalues with EoS of hessence being $-1 + \lambda^2/3$ and total EoS also being $-1 + \lambda^2/3$ (i.e., both EoS are "quintessence-like" if $\lambda^2 < 3$ or "dust-like" if $\lambda^2 = 3$). The graphs in Figures 8 and 9 also support the fact corresponding to the stable manifolds. For $\lambda = -0.5$, the EoS of hessence and total EoS both behave like "quintessence."

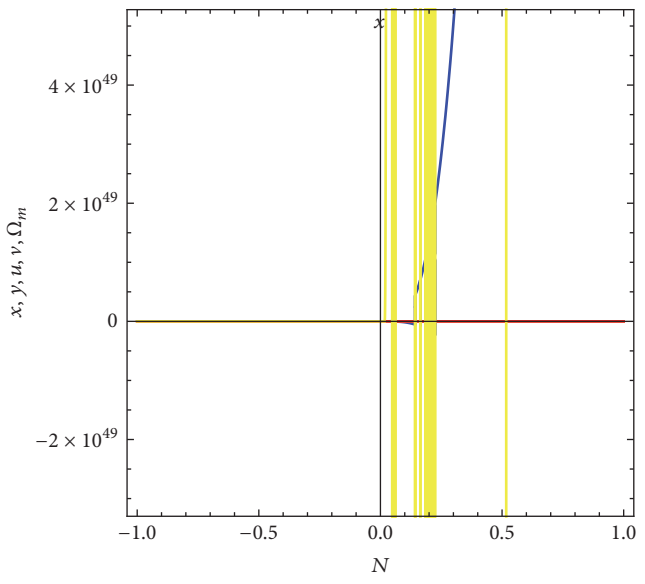

FIGURE 10: Plot of (10) variations of x (blue), y (green), u (orange), v (red), and Ω_m (yellow) versus N near P_{11}, for $\gamma = 1$, $\delta = 1$, and $\lambda = -0.5$. The position corresponding to $N = 0$ is the fixed point under consideration.

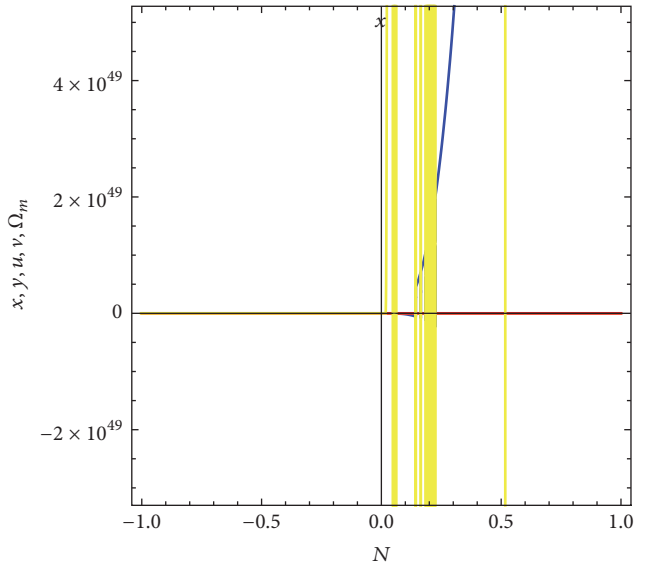

FIGURE 11: Plot of (11) variations of x (blue), y (green), u (orange), v (red), and Ω_m (yellow) versus N near P_{12}, for $\gamma = 1$, $\delta = 1$, and $\lambda = -0.5$. The position corresponding to $N = 0$ is the fixed point under consideration.

We note that if $a^2 + b^2/2 \leq 1, D \leq -\sqrt{\Delta}$ (equality should occur in one of them), P_{11} and P_{12} may admit 3-dimensional stable manifold corresponding to the negative eigenvalues with EoS of hessence being $(-1 + 2A^2 + B^2)/(1 - B)$ and total EoS being $-1 + A^2 + B^2 + (\gamma - 2)B$. We see from Figure 10 that the system is moving away from the fixed point P_{11}. Similar phenomena happen for fixed point P_{12} as seen from Figure 11.

We note that if $2\delta < \lambda < 0$ or $0 < \lambda < 2\delta$, then P_{13} and P_{14} may admit 1-dimensional stable manifold corresponding

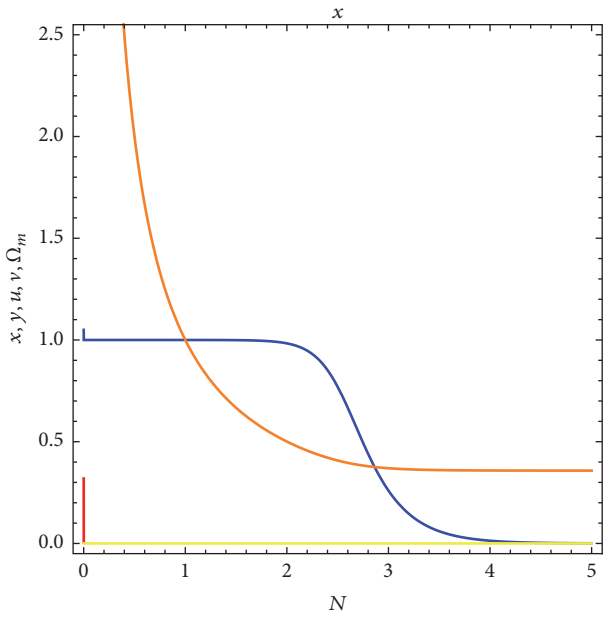

FIGURE 12: Plot of (12) variations of x (blue), y (green), u (orange), v (red), and Ω_m (yellow) versus N near P_{13}, for $\gamma = 1$, $\delta = 1$, and $\lambda = -0.5$. The position corresponding to $N = 0$ is the fixed point under consideration.

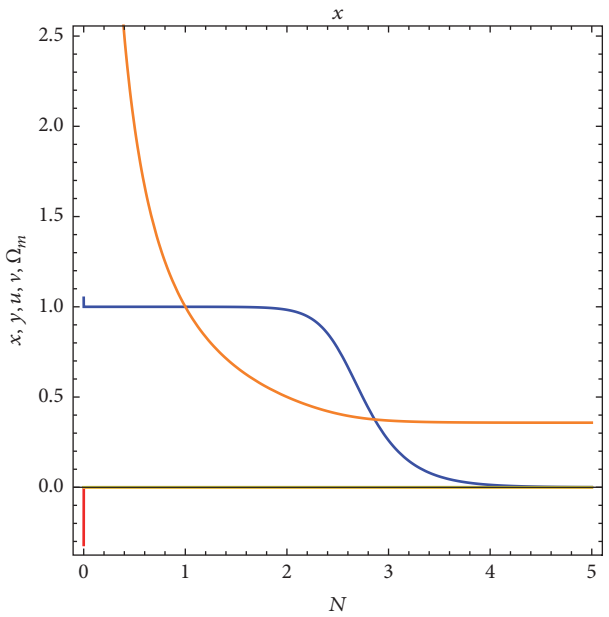

FIGURE 13: Plot of (13) variations of x (blue), y (green), u (orange), v (red), and Ω_m (yellow) versus N near P_{14}, for $\gamma = 1$, $\delta = 1$, and $\lambda = -0.5$. The position corresponding to $N = 0$ is the fixed point under consideration.

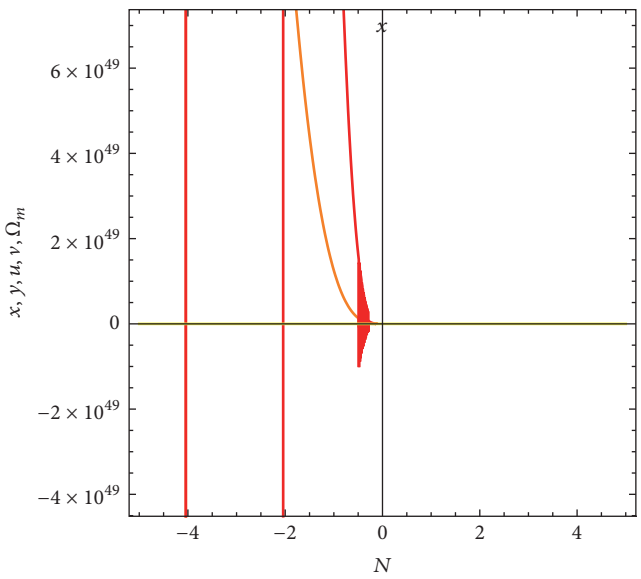

FIGURE 14: Plot of (14) variations of x (blue), y (green), u (orange), v (red), and Ω_m (yellow) versus N near P_{15}, for $\gamma = 1$, $\delta = 1/(4\sqrt{6})$, and $\lambda = -0.5$. The position corresponding to $N = 0$ is the fixed point under consideration.

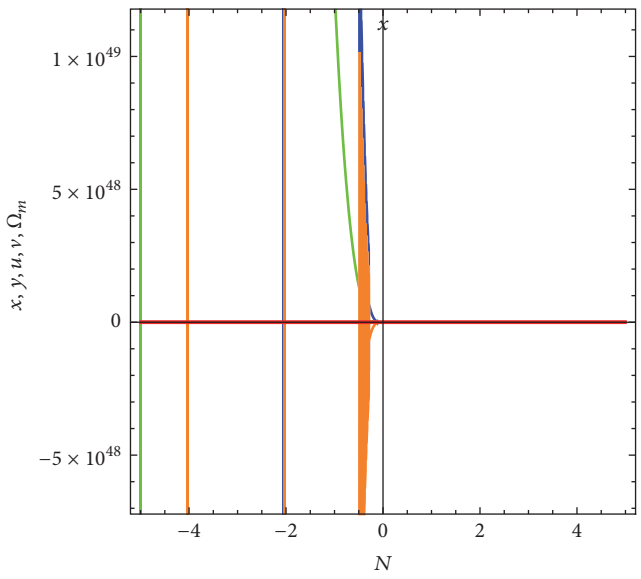

FIGURE 15: Plot of (15) variations of x (blue), y (green), u (orange), v (red), and Ω_m (yellow) versus N near P_{16}, for $\gamma = 1$, $\delta = 1/(4\sqrt{6})$, and $\lambda = -0.5$. The position corresponding to $N = 0$ is the fixed point under consideration.

to the negative eigenvalues with EoS of hessence and total EoS being 1 and universe decelerates. The graphs in Figures 12 and 13 show that the system is diverging from the fixed points P_{13} and P_{14}. So, both the points are unstable in nature.

We note that if $x\delta \leq -\sqrt{3/2}$ and $x\lambda \leq -\sqrt{6}$, then P_{15} and P_{16} may admit 2-dimensional stable manifold corresponding to the two negative eigenvalues with EoS of hessence and total EoS being 1 and universe decelerates. Here, we note that the solution set of the dynamical system moves rapidly from the fixed points P_{15} and P_{16} as clear from Figures 14 and 15. The fixed points are unstable.

5. Cosmological Significance of the Fixed Points

In this section, we discuss the possible singularities that any dark energy model could have and compare the fixed points against recent dataset's, Planck 2015, data [27]. If the EoS $\omega \leq -1$ (i.e., the null energy condition $p + \rho \geq 0$ is violated) and Big Rip singularity happen within a finite time [20], this singularity happens when, at finite time $t \to t_s$, $a \to \infty$, $\rho \to \infty$, and $|p| \to \infty$.

We now analyse the stable fixed points to see if they can avoid (or suffer) Big Rip singularity. For the stable fixed points P_7 and P_8, we have $\dot{H}/H^2 = 0$ which gives $H = k$ (the integral constant); we get $a \propto e^{kt}$. Also, in these cases, $\omega_{\text{total}} = -1$ which with energy conservation equation gives $\rho =$ constant. Hence universe suffers no Big Rip singularity here. Fixed points P_7 and P_8 exist with physical parameters $\Omega_m = 0$, $\omega_h = -1$, and $\omega_{\text{total}} = -1$. The values of the parameters are well within the best fit of Planck 2015 data; that is, $\Omega_m = 0.3089 \pm 0.0062$ from TT,TE,EE + lowP + lensing + ext data, and EoS of dark energy $\omega = -1.019^{+0.075}_{-0.080}$.

Now, we consider the unstable fixed points. An unstable fixed point may describe the initial phase of universe, whereas a stable fixed point may be the end phase of the universe. For fixed points P_1, P_2, and P_3 existing with the physical parameters $\Omega_m = 0$, $\omega_h = 1$, and $\omega_{\text{total}} = 1$, clearly, no Big Rip singularity occurs here. Here, the parameter Ω_m lies within the best fit of Planck 2015 data; that is, $\Omega_m = 0.3089 \pm 0.0062$ from TT,TE,EE + lowP + lensing + ext data. But ω_h and ω_{total} defy the EoS of dark energy $\omega = -1.019^{+0.075}_{-0.080}$.

Fixed point P_4 has values of physical parameters $\Omega_m = (6 - 3\gamma + 2\delta^2)/3$, $\omega_h = 1$, and $\omega_{\text{total}} = -1 + \gamma(1 - 2\delta^2/3) + 4\delta^2/3$. Here, ω_h and ω_{total} both are greater than -1; no Big Rip singularity occurs here too. Wide choices of γ and δ can fit Ω_m and ω_{total} within Planck 2015 data; that is, $\Omega_m = 0.3089 \pm 0.0062$, but ω_h disobey the EoS of dark energy $\omega = -1.019^{+0.075}_{-0.080}$.

Fixed points P_5 and P_6 exist with physical parameters $\Omega_m = 0$, $\omega_h = 1$, and $\omega_{\text{total}} = 1$. We observe that this solution is devoid of Big Rip singularity. Here, Ω_m lies within the best fit of Planck 2015 data. But ω_h and ω_{total} defy the EoS of dark energy $\omega = -1.019^{+0.075}_{-0.080}$.

Fixed points P_9 and P_{10} admit physical parameters as $\Omega_m = 0$, $\omega_h = -1 + \lambda^2/3$, and $\omega_{\text{total}} = -1 + \lambda^2/3$ and so avoid Big Rip singularity. Also, Ω_m is within Planck 2015 data. Also, suitable choice of λ fits ω_h and ω_{total} within dataset.

Fixed points P_{11} and P_{12} have physical parameters $\Omega_m = B$, $\omega_h = (-1+2A^2+B^2)/(1-B)$, and $\omega_{\text{total}} = -1+A^2+B^2+(\gamma-2)B$, where $A = -\sqrt{3/2}(\gamma/(\delta+\lambda))$ and $B = (6+\lambda\sqrt{6}A-6A^2)/9$. Here, we can adjust A and B to make ω_h and $\omega_{\text{total}} \geq -1$ miss Big Rip singularity. Since only $0 < \gamma \leq 2$, δ can take arbitrary small value and λ can have any real value, A, and hence B can be adjusted well within Planck $\Omega_m = 0.3089 \pm 0.0062$ from TT,TE,EE + lowP + lensing + ext and EoS of dark energy $\omega = -1.019^{+0.075}_{-0.080}$ data.

Fixed points P_{13}, P_{14}, P_{15}, and P_{16} can avoid Big Rip singularity, as they bear physical parameters $\Omega_m = 0$, $\omega_h = 1$, and $\omega_{\text{total}} = 1$. Here, the parameter Ω_m lies within the best fit of Planck 2015 data; that is, $\Omega_m = 0.3089 \pm 0.0062$ from TT,TE,EE + lowP + lensing + ext data. But ω_h and ω_{total} totally defy the EoS of dark energy $\omega = -1.019^{+0.075}_{-0.080}$.

6. Concluding Remarks

In this paper, we have performed a dynamical system study of a unique scalar field hessence coupling with dark matter in an alternate theory of gravity, namely, $f(T)$ gravity. The system is unconventional, complex, but quite interesting. The model is chosen to explore one of the various possibilities about the fate of the universe. The sole purpose is to explain the current acceleration of universe. An unstable fixed point may describe the initial phase of universe, whereas a stable fixed point may be the end of the universe. We have chosen exponential form of potential of the form $V = V_0 e^{\lambda\phi}$ (where V_0 and λ are real constants and ϕ is the hessence field) for simplicity. The interaction term C is chosen to solve the so-called cosmological constant problem in tune with second law of thermodynamics and is quite arbitrary (only C should remain positive), since $C = \delta\dot{\phi}\rho_m$, where δ is a real constant of small magnitude, which may be chosen as positive or negative, such that C remains positive. Also, $\dot{\phi}$ may be positive or negative according to the hessence field ϕ. The resulting nonlinear dynamical system gives sixteen possible fixed points. Among them, P_7 and P_8 are stable set of normally hyperbolic fixed points, which resembles "cosmological constant," so it explains the current phase of acceleration of universe. But, interestingly, it does not show "hessence-like" nature. Among the other fixed points, the initial phases of evolution may begin. However, the complexity of the system is the main obstacle for a precise explanation. Anyway, in future work, we may try some other possible alternatives.

Conflicts of Interest

The authors declare that there are no conflicts of interest regarding the publication of this paper.

Acknowledgments

One of the authors (Ujjal Debnath) is grateful to IUCAA, Pune, India, where part of the work was carried out, for warm hospitality.

References

[1] A. G. Riess, L.-G. Strolger, and J. Tonry, "Type Ia supernova discoveries at $z > 1$ from the *Hubble Space Telescope*: evidence for past deceleration and constraints on dark energy evolution," *The Astrophysical Journal*, vol. 607, no. 2, pp. 665–687, 2004.

[2] R. A. Knop, G. Aldering, R. Amanullah et al., "New constraints on Ω_M, Ω_Λ, and w from an independent set of 11 high-redshift supernovae observed with the *Hubble Space Telescope*," *The Astrophysical Journal*, vol. 598, no. 1, p. 102, 2003.

[3] P. Astier, J. Guy, N. Regnault et al., "The Supernova Legacy Survey: measurement of Ω_M, Ω_Λ and w from the first year data set," *Astronomy & Astrophysics*, vol. 447, no. 1, Article ID 0510447, pp. 31–48, 2006.

[4] J. D. Neill, M. Sullivan, D. Balam et al., "The type Ia supernova rate at $Z \approx 0.5$ from the supernova legacy survey," *The Astronomical Journal*, vol. 132, no. 3, 2006.

[5] C. L. Bennett, M. Halpern, G. Hinshaw et al., "First-year wilkinson microwave anisotropy probe (wmap) observations: preliminary maps and basic results," *The Astrophysical Journal*, vol. 148, no. 1, Article ID 0302207, 2003.

[6] D. N. Spergell, L. Verde, H. V. Peiris et al., "First-year Wilkinson microwave anisotropy probe (wmap) observations: determination of cosmological parameters," *The Astrophysical Journal Supplement Series*, vol. 148, no. 1, pp. 175–194, 2003.

[7] D. N. Spergell, R. Bean, O. Doré et al., "Three-year Wilkinson microwave anisotropy probe (wmap) observations: implications for cosmology," *The Astrophysical Journal*, vol. 170, no. 2, p. 377, 2007.

[8] L. Page, G. Hinshaw, E. Komatsu et al., "Three year wilkinson microwave anisotropy probe (WMAP) observations: polarization analysis," *The Astrophysical Journal*, vol. 170, no. 2, p. 335, 2007.

[9] G. Hinshaw, M. R. Nolta, C. L. Bennett et al., "Three-year wilkinson microwave anisotropy probe (wmap) observations: temperature analysis," *The Astrophysical Journal*, vol. 170, no. 2, p. 288, 2007.

[10] N. Jarosik, C. Barnes, M. R. Greason et al., "Three-year wilkinson microwave anisotropy probe (WMAP) observations: beam profiles, data processing, radiometer characterization, and systematic error limits," *The Astrophysical Journal*, vol. 170, no. 2, p. 263, 2007.

[11] E. Komatsu, "[WMAP collaboration]," *Astrophysics J. Suppl*, vol. 192 18, 2011.

[12] M. Tegmark et al., "Cosmological parameters from SDSS and WMAP," *Physical Review D*, vol. 69, Article ID 103501, 2004.

[13] M. Tegmark, M. R. Blanton, M. A. Strauss, F. Hoyle, and D. Schlegel, "The three-dimensional power spectrum of galaxies from the sloan digital sky survey," *The Astrophysical Journal*, vol. 606, no. 2, p. 702, 2004.

[14] U. Seljak, A. Makarov, P. McDonald et al., "Cosmological parameter analysis including SDSS Lyα forest and galaxy bias: Constraints on the primordial spectrum of fluctuations, neutrino mass, and dark energy," *Physical Review D*, vol. 71, Article ID 103515, 2005.

[15] J. K. Adelman-McCarthy, M. A. Agüeros, S. S. Allam et al., "The fourth data release of the sloan digital sky survey," *The Astrophysical Journal*, vol. 162, no. 1, Article ID 0507711, 2006.

[16] M. Tegmark, M. R. Blanton, and M. l. A. Strauss, "The three-dimensional power spectrum of galaxies from the sloan digital sky survey," *The Astrophysical Journal*, vol. 606, no. 2.

[17] M. Tegmark, D. Eisenstein, M. Strauss et al., "Cosmological constraints from the SDSS luminous red galaxies," *Physical Review D*, vol. 74, Article ID 123507, 2006.

[18] S. W. Allen, R. W. Schmidt, H. Ebeling, A. C. Fabian, and L. Van Speybroeck, "Constraints on dark energy from *Chandra* observations of the largest relaxed galaxy clusters," *Monthly Notices of the Royal Astronomical Society*, vol. 353, p. 457, 2004.

[19] A. G. Riess, L.-G. Strolger, S. Casertano et al., "New *hubble space telescope* discoveries of type Ia supernovae at $Z \geq 1$ narrowing constraints on the early behavior of dark energy," *The Astrophysical Journal*, vol. 1, 659.

[20] E. J. Copeland, M. Sami, and S. Tsujikawa, "Dynamics of dark energy," *International Journal of Modern Physics D: Gravitation, Astrophysics, Cosmology*, vol. 15, no. 11, pp. 1753–1935, 2006.

[21] S. Weinberg, "The cosmological constant problem," *Reviews of Modern Physics*, vol. 61, no. 1, pp. 1–23, 1989.

[22] P. J. Peebles and B. Ratra, "The cosmological constant and dark energy," *Reviews of Modern Physics*, vol. 75, no. 2, pp. 559–606, 2003.

[23] T. Padmanabhan, "Dark energy: the cosmological challenge of the millennium," *Current Science*, vol. 88, p. 1057, 2005.

[24] J. Martin and M. Yamaguchi, "DBI-essence," *Physical Review D*, vol. 77, Article ID 123508, 2008.

[25] L. P. Chimento, R. Lazkoz, and I. Sendra, "DBI models for the unification of dark matter and dark energy," *General Relativity and Gravitation*, vol. 42, no. 5, pp. 1189–1209, 2010.

[26] P. A. R. Ade, N. Aghanim, C. Armitage-Caplan et al., "Planck 2013 results. XVI. Cosmological parameters," *Astronomy & Astrophysics*, vol. 571, no. A16, 66 pages, 2013.

[27] P. A. R. Ade, N. Aghanim, M. Arnaud et al., "Planck 2015 results. XIII. Cosmological parameters," *Astronomy & Astrophysics*, vol. 594, article A13, 63 pages, 2016.

[28] A. Albrecht and P. J. Steinhardt, "Cosmology for grand unified theories with radiatively induced symmetry breaking," *Physical Review Letters*, vol. 48, p. 1220, 1982, A complete description of inflationary models can be found in the book by A. Linde, Particle Physicss and Inflationary Cosmology, Gordon and Breach, New York U.S.A. (1990).

[29] A. H. Guth, "Inflationary universe: a possible solution to the horizon and flatness problems," *Physical Review D*, vol. 23, p. 347, 1981.

[30] A. Berera, I. J. Moss, and R. O. Ramos, *Reports on Progress in Physics*, vol. 70, Article ID 026901, 2009.

[31] A. Berera and L.-Z. Fang, "Thermally induced density perturbations in the inflation era," *Physical Review Letters*, vol. 74, no. 11, pp. 1912–1915, 1995.

[32] A. Berera, *Physical Review Letters*, vol. 75, p. 3218, 1995, ; Physical Review D, vol. 55, p. 3346, 1997.

[33] P. Steinhardt, *Critical Problems in Physics*, Princeton University Press, Princeton, NJ, USA, 1997.

[34] I. Zlatev, L. Wang, and P. J. Steinhardt, "Quintessence, cosmic coincidence, and the cosmological constant," *Physical Review Letters*, vol. 82, no. 5, pp. 896–899, 1999.

[35] S. M. Carrol, "Quintessence and the rest of the world: suppressing long-range interactions," *Physical Review Letters*, vol. 81, p. 3067, 1998.

[36] U. Alam, V. Sahni, T. D. Saini, and A. A. Starobinsky, "Is there supernova evidence for dark energy metamorphosis?" *Monthly Notices of the Royal Astronomical Society*, vol. 354, no. 1, pp. 275–291, 2004.

[37] R. R. Caldwell, "A phantom menace? Cosmological consequences of a dark energy component with super-negative equation of state," *Physics Letters B*, vol. 545, no. 1-2, pp. 23–29, 2002.

[38] R. R. Caldwell, M. Kamionkowski, and N. N. Weinberg, "Phantom energy: dark energy with $\omega < -1$ causes a cosmic doomsday," *Physical Review Letters*, vol. 91, Article ID 071301, 2003.

[39] R. J. Scherrer, "Phantom dark energy, cosmic doomsday, and the coincidence problem," *Physical Review D*, vol. 71, Article ID 063519, 2005.

[40] L. P. Chimento, M. I. Forte, R. Lazcoz, and M. G. Richarte, "Internal space structure generalization of the quintom cosmological scenario," *Physical Review D*, vol. 79, Article ID 0435002, 2009.

[41] B. Feng, X. L. Wang, and X. M. Zhang, "Dark energy constraints from the cosmic age and supernova," *Physics Letters B*, vol. 607, no. 35, 2005.

[42] L. A. Boyle, R. R. Caldwell, and M. Kamionkowski, "Spintessence! New models for dark matter and dark energy," *Physics Letters, Section B: Nuclear, Elementary Particle and High-Energy Physics*, vol. 545, no. 1-2, pp. 17–22, 2002.

[43] S. Kasuya, "Difficulty of a spinning complex scalar field to be dark energy," *Physics Letters B*, vol. 515, no. 1-2, pp. 121–124, 2001.

[44] H. Wei, R.-G. Cai, and D.-F. Zeng, "Hessence: a new view of quintom dark energy," *Classical and Quantum Gravity*, vol. 22, no. 16, pp. 3189–3202, 2005.

[45] H. Wei and R-G. Cai, "Cosmological evolution of "hessence" dark energy and avoidance of the big rip," *Physical Review D*, vol. 72, Article ID 123507, 2005.

[46] M. Alimohammadi and H. M. Sadjadi, "Attractor solutions for general hessence dark energy," *Physical Review D*, vol. 73, Article ID 083527, 2006.

[47] H. Wei, N. Tang, and S. N. Zhang, "Reconstruction of hessence dark energy and the latest typeIa supernovae gold dataset," *Physical Review D*, vol. 75, Article ID 043009, 2007.

[48] S. Capozziello and L. Z. Fang, "International Journal of Modern Physics D," *Curvature Quintessence*, vol. 11, no. 4, pp. 483–491, 2002.

[49] S. Nojiri and S. D. Odintsov, "Modified gravity with negative and positive powers of curvature: unification of inflation and cosmic acceleration," *Physical Review D*, vol. 68, Article ID 123512, 2003.

[50] S. M. Carroll, V. Duvvuri, M. Trodden, and M. S. Turner, "Is cosmic speed-up due to new gravitational physics?" *Physical Review D*, vol. 70, Article ID 043528, 2004.

[51] A. Einstein, "Riemannian geometry with maintaining the notion of distant parallelism," *Preuss. Akad. Wiss., Phys.-Math. Ki*, vol. 217, 1928.

[52] A. Einstein, "A unified field theory based on the riemannian metric and distant parallelism," *Mathematische Annalen*, vol. 102, p. 685, 1930.

[53] K. Hayashi and T. Shirafuji, "New general relativity," *Physical Review D: Particles and Fields*, vol. 19, no. 12, pp. 3524–3553, 1979.

[54] R. Aldrovandi and J. G. Pereira, *Teleparallel Gravity: An Introduction*, vol. 173, Springer, New York, NY, USA, 2013.

[55] M. P. Gaugh, "Beyond LCDM: a viable alternative?" https://arxiv.org/abs/1607.00330.

[56] A. Behboodi, S. Akshabi, and K. Nozari, "Matter stability in modified teleparallel gravity," *Physics Letters B*, vol. 718, no. 1, pp. 30–33, 2012.

[57] E. Dil and E. Kolay, "Dynamics of mixed dark energy domination in teleparallel gravity and phase-space analysis," *Advances in High Energy Physics*, vol. 2015, Article ID 608252, 20 pages, 2015.

[58] R. Lazcoz, G. Leon, and I. Quiros, "Quintom cosmologies with arbitrary potentials".

[59] H. Wei and S. N. Zhang, "Dynamics of quintom and hessence energies in loop quantum cosmology," *Physical Review D*, vol. 76, no. 6, Article ID 063005, 2007.

[60] S. K. Biswas and S. Chakraborty, "Interacting dark energy in $f(T)$ cosmology: a dynamical system analysis," *International Journal of Modern Physics. D. Gravitation, Astrophysics, Cosmology*, vol. 24, no. 7, 1550046, 20 pages, 2015.

[61] E. E. Flanagan and E. Rosenthal, "Can gravity probe B usefully constrain torsion gravity theories?" *Physical Review D*, vol. 75, Article ID 124016, 2007.

[62] J. Garecki, "Teleparallel equivalent of general relativity: a critical review," https://arxiv.org/abs/1010.2654.

[63] G. R. Bengochea and R. Ferraro, "Dark torsion as the cosmic speed-up," *Physical Review D*, vol. 79, Article ID 124019, 2009.

[64] E. V. Linder, "Einstein*ı*s other gravity and the acceleration of the universe," *Physical Review D*, vol. 81, Article ID 127301, 2010, [Erratum-*ibid*D**82**, 109902 (2010)].

[65] P. Wu and H. Yu, "Observational constraints on $f(T)$ theory," *Physics Letters B*, vol. 693, no. 4, pp. 415–420, 2010.

[66] P. Wu and H. Yu, "$f(T)$ models with phantom divide line crossing," *The European Physical Journal C*, vol. 71, p. 1552, 2011.

[67] M. R. Setare and M. J. S. Houndjo, "Finite-time future singularities models in *f(T)* gravity and the effects of viscosity," *Canadian Journal of Physics*, vol. 91, no. 3, pp. 260–267, 2013.

[68] M. H. Daouda, M. E. Rodrigues, and M. J. S. Houndjo, "Reconstruction of $f(T)$ gravity according to holographic dark energy," *The European Physical Journal C*, vol. 72, article 1893, 2012.

[69] V. F. Cardone, N. Radicella, and S. Camera, "Accelerating $f(T)$ gravity models constrained by recent cosmological data," *Physical Review D*, vol. 85, Article ID 124007, 2012.

[70] S. Camera, V. F. Cardone, and N. Radicella, "Detectability of torsion gravity via galaxy clustering and cosmic shear measurements," *Physical Review D*, vol. 89, Article ID 083520, 2014.

[71] K. Bamba, M. Jamil, D. Momeni, and R. Myrzakulov, "Generalized second law of thermodynamics in *f(T)* gravity with entropy corrections," *Astrophysics and Space Science*, vol. 344, no. 1, pp. 259–267, 2013.

[72] G. Dvali, G. Gabadadze, and M. Porrati, "4D gravity on a brane in 5D MInkowski space," *Physics Letters. B. Particle Physics, Nuclear Physics and Cosmology*, vol. 485, no. 1-3, pp. 208–214, 2000.

[73] C. Deffayet, G. Dvali, and G. Gabadadze, "Accelerated universe from gravity leaking to extra dimensions," *Physical Review. D. Third Series*, vol. 65, no. 4, Article ID 044023, 9 pages, 2002.

[74] K. Nozari and N. Behrouz, "An interacting dark energy model with nonminimal derivative coupling," *Physics of the Dark Universe*, vol. 13, no. 92, 2016.

[75] N. Mahata and S. Chakraborty, "A Dynamical System Analysis of Three Fluid cosmological Model," https://arxiv.org/abs/1512.07017.

[76] J. Wainwright and G. F. R. Ellis, *Dynamical Systems in Cosmology*, Cambridge University Press, Cambridge, UK, 1997.

[77] B. Aulbach, *Continuous and Discrete Dynamics Near Manifolds of Equilibria*, vol. 1058 of *Lecture Notes in Mathematics*, Springer-Verlag, Berlin, Germany, 1984.